

# Vortex knots in a Bose-Einstein condensate

Davide Proment,<sup>1,2,\*</sup> Miguel Onorato,<sup>1,2</sup> and Carlo F. Barenghi<sup>3</sup>

<sup>1</sup>*Dipartimento di Fisica Generale, Università degli Studi di Torino,*

*Via Pietro Giuria 1, 10125 Torino, Italy, EU*

<sup>2</sup>*INFN, Sezione di Torino, Via Pietro Giuria 1, 10125 Torino, Italy, EU*

<sup>3</sup>*School of Mathematics and Statistics, Newcastle University,*

*Newcastle upon Tyne, NE1 7RU, UK, EU*

(Dated: October 21, 2018)

## Abstract

We present a method for numerically building a vortex knot state in the superfluid wave-function of a Bose-Einstein condensate. We integrate in time the governing Gross-Pitaevskii equation to determine evolution and stability of the two (topologically) simplest vortex knots which can be wrapped over a torus. We find that the velocity of a vortex knot depends on the ratio of poloidal and toroidal radius: for smaller ratio, the knot travels faster. Finally, we show how unstable vortex knots break up into vortex rings.

PACS numbers:

47.32.C- Vortex dynamics (fluid flow);

03.75.Lm Vortices in Bose-Einstein condensation;

Keywords: Vortex dynamics; Bose-Einstein condensate; knot theory

---

\* [davideproment@gmail.com](mailto:davideproment@gmail.com); [www.to.infn.it/~proment](http://www.to.infn.it/~proment)

## I. INTRODUCTION

In 1867, following the works of Helmholtz on vortices and of Riemann on abelian functions, Lord Kelvin modelled atoms as knotted vortex tubes in the ether [1], effectively giving birth to knot theory [2]. This discipline has fascinated mathematicians and physicists since. More recently, knots have been studied in different branches of physics, ranging from excitable media [3], and classical field theory [4], to optics [5, 6] and liquid-crystal colloids [7].

Knots in superfluids are identified with closed vortex lines, regions of fluid around which the circulation assumes non-zero (quantized) value. Vortex rings have been studied experimentally in superfluid liquid helium [8, 9] and in Bose-Einstein condensates [10]. Numerical simulations have revealed that superfluid turbulence contains linked vortex lines [11], but, to the best of our knowledge, individual vortices with non-trivial topology have never been observed directly. To shed light onto this problem, energy, motion and stability of vortex knots have been examined theoretically and numerically using the classical theory of thin-cored vortex filaments. In this approach, the governing incompressible Euler dynamics is expressed by the Biot-Savart law or by its local induction approximation (LIA) [12, 13]. Under certain conditions, it is found that some vortex knots are structurally stable, that is to say they travel without breaking up for distance larger than their own diameters.

In superfluid helium, the validity of the classical theory of thin-core vortex filaments is based on the large separation of scales between the vortex core radius  $a_0$  (approximately  $10^{-8}$  cm in  $^4\text{He}$  and  $10^{-6}$  cm in  $^3\text{He-B}$ ) and the typical distance  $\ell$  between vortices. In turbulence experiments,  $\ell \approx 10^{-3}$  to  $10^{-4}$  cm; the last value is also the typical diameter of experimental vortex rings [9]. The situation is very different in atomic Bose-Einstein condensates, where  $\ell$  is only few times larger than  $a_0$ . In this context, the Gross-Pitaevskii Equation (GPE) is clearly a more realistic model [14], particularly at very low temperatures, as thermal effects can be neglected.

The advantage of the GPE is that it does not need the cut-off parameter required by the classical vortex filament theory to de-singularise the Biot-Savart integral [15]. The second advantage is that the GPE naturally describes vortex reconnections [16], which must be implemented algorithmically in the Biot-Savart model. Any prediction about the stability and the break-up of a vortex structure which is not orders of magnitude bigger than  $a_0$  is therefore more reliable if obtained using the GPE. The third advantage of searching for vortex

knots in a Bose-Einstein condensate is that direct images of individual vortex structures are possible without the use of tracer particles which will certainly disturb these structures. The disadvantage is that atomic condensates are small, thus the motion of these structures will be affected by the boundaries and by the non-uniformity density of the background condensate. Before investigating these effects, however, it is essential to establish whether vortex knot solutions of the governing GPE exist, and, if they do, if they are sufficiently stable. This is the limited aim which we set in this work. We stress that we do not aim to propose a mechanism to experimentally create vortex knots in condensates, but only to study the possible existence and stability of these solutions of the GPE. We shall see that even setting up numerically a topologically non-trivial structure in the wave-function is not a minor task; indeed, to the best of our knowledge, this is the first time it has been done.

The manuscript is organized as the following. Section II explains how to create an elementary vortex knot in the initial conditions of the condensate wave-function. Section III deals with the analysis of the dynamical properties of vortex knots. Section IV describes the break-up of vortex knots. Finally, the conclusions are in Section V.

## II. VORTEX KNOT INITIAL CONDITIONS

We consider the GPE written in the following dimensionless form

$$2i \partial_t \psi - \nabla^2 \psi + |\psi|^2 \psi = 0, \quad (1)$$

where no external confining potential is present. The characteristic length scale of perturbations of the uniform condensate, called *healing length*, is defined as

$$\xi = \frac{1}{\sqrt{\langle \rho \rangle}}, \quad \text{where } \langle \rho \rangle = \frac{1}{V} \int_V |\psi|^2 dV \quad (2)$$

is the mean density of the condensate. Besides the energy, the GPE conserves the total number of particles, therefore  $\xi$  is a conserved quantity too. Without loss of generality, we choose to deal with a system that has an unperturbed density (the density field at infinity) equal to unity, and assume that perturbations are localized in a small region of the sample. In this hypothesis,  $\xi \simeq 1$  in our units.

We now explain how to numerically build a vortex knot. First we construct a vortex. Consider the two dimensional plane  $sOz$ . A stable vortex is a hole (zero value) in the density

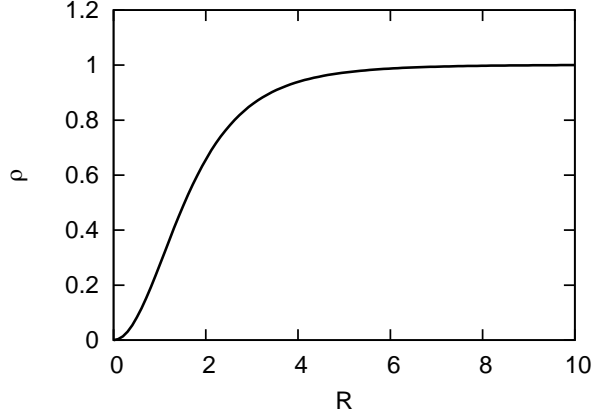


FIG. 1. (Colours online). The density field  $\rho$  around an axisymmetric two-dimensional vortex. Radial distances  $R$  are in units of the healing length  $\xi$ .

field, around which the phase of the wave-function changes by  $\pm 2\pi$ . A sufficiently accurate description of a two-dimensional vortex centered in the origin of the  $sOz$  plane is given by the wave-function  $\Psi_{2D}(s, z) = \sqrt{\rho(R)} e^{i\theta(s, z)}$ , where  $R = \sqrt{s^2 + z^2}$ ,

$$\begin{aligned} \rho(R) &= \frac{R^2 (a_1 + a_2 R^2)}{1 + b_1 R^2 + b_2 R^4}, \\ \theta(s, z) &= \arctan\left(\frac{z}{s}\right), \end{aligned} \quad (3)$$

and the coefficients  $a_1 = 11/32$ ,  $a_2 = 11/384$ ,  $b_1 = 1/3$ , and  $b_2 = 11/384$  arise from a second order Padé approximation [17]. Fig. 1 shows how the density field behaves around the axisymmetric vortex centre. It is clear from the plot that the vortex core is of the order of the healing length, and the bulk value of the density  $\rho = 1$  is recovered at larger distances.

We now come back to vortex knots in a three-dimensional system. We define a knot as a closed curve over a torus, characterized by the toroidal radius  $R_0$  and the poloidal radius  $R_1$ . More precisely, a closed curve  $\mathcal{T}_{n,m}$  on the torus is determined by counting the number of toroidal wraps,  $n$ , and the number of poloidal wraps,  $m$ . For example, the curves  $\mathcal{T}_{1,1}$  and  $\mathcal{T}_{2,2}$  describe respectively the unknot (the simple vortex ring) and two unlinked rings. The first topologically non-trivial curve is the trefoil,  $\mathcal{T}_{2,3}$ . In this work we shall focus on the two simplest knots, the trefoil  $\mathcal{T}_{2,3}$  and its dual  $\mathcal{T}_{3,2}$ .

### A. The $\mathcal{T}_{2,3}$ knot (trefoil)

The vortex line of a  $\mathcal{T}_{2,3}$  knot lays on the torus as shown in Fig. 2. Any plane  $sOz$  passing

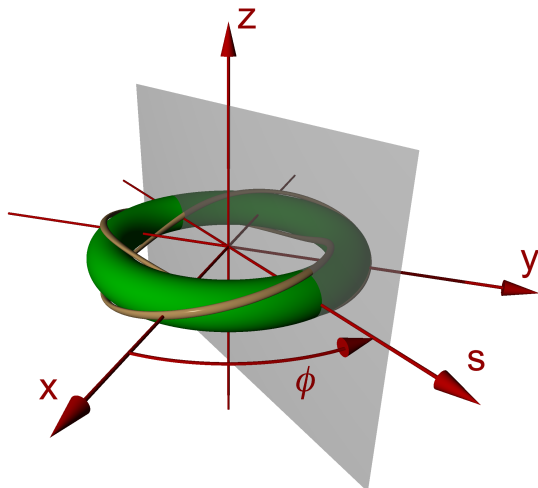


FIG. 2. (Colours online). Construction of the trefoil knot  $\mathcal{T}_{2,3}$ .

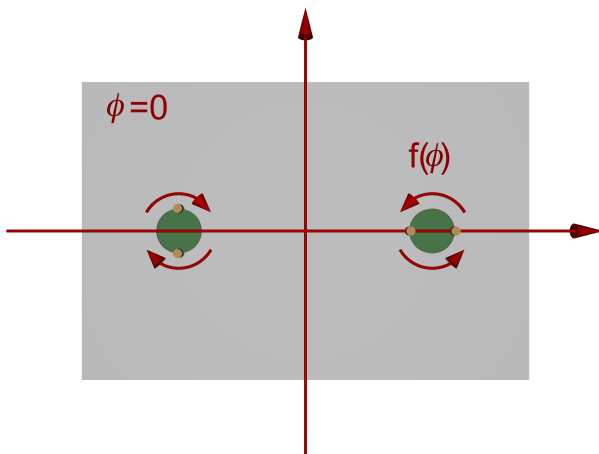


FIG. 3. (Colours online). Positions of the four vortices on  $\phi = 0$  used to construct the wave-function of the trefoil knot  $\mathcal{T}_{2,3}$ .

through the  $z$  axis intercepts the curve  $\mathcal{T}_{2,3}$  at four different points, which correspond to four two-dimensional point vortices on the plane  $sOz$ . The positions of these two-dimensional vortices vary with respect to the choice of the plane  $sOz$ ; in other words, these positions are functions of the angle variable  $\phi$  introduced in Fig. 2. For example, the vortex positions of the wave-function for the angle  $\phi = 0$  are shown in Fig. 3. By construction, these point vortices are located on the circumference defined by the intersection of the plane with the torus, and rotate on it following a particular function  $f(\phi)$ . To assure continuity of the vortex line and to describe the trefoil knot, the function  $f(\phi)$  must have the form  $f(\phi) = 3\phi/2$ ,

with  $\phi \in [0, \pi)$ .

We are now ready to write the three-dimensional wave-function which describes the trefoil knot  $\mathcal{T}_{2,3}$ . In the approximation that the healing length  $\xi$  is much smaller than the inter-vortex distance, the two-dimensional wave-function in the plane  $sOz$  is given by the superposition (multiplication) of the wave-function  $\Psi_{2D}$  of each two-dimensional vortex centered in the correct position, where the opposite circulation is obtained by applying the complex conjugation operator  $(...)^*$ . Thus, the three-dimensional wave-function results in

$$\begin{aligned}
\psi_{2,3}(x, y, z) = & \Psi_{2D} \{s(x, y) - R_0 - R_1 \cos [\alpha(x, y)], z - R_1 \sin [\alpha(x, y)]\} \\
& \times \Psi_{2D} \{s(x, y) - R_0 - R_1 \cos [\alpha(x, y) + \pi], z - R_1 \sin [\alpha(x, y) + \pi]\} \\
& \times \Psi_{2D}^* \{s(x, y) + R_0 - R_1 \cos [\alpha(x, y) + \pi/2], z + R_1 \sin [\alpha(x, y) + \pi/2]\} \\
& \times \Psi_{2D}^* \{s(x, y) + R_0 - R_1 \cos [\alpha(x, y) + 3\pi/2], z + R_1 \sin [\alpha(x, y) + 3\pi/2]\},
\end{aligned} \tag{4}$$

with  $s(x, y) = \text{sgn}(x)\sqrt{x^2 + y^2}$ , where  $\text{sgn}(\dots)$  is the sign function, and  $\alpha(x, y) = 3/2 \arctan (y/x)$ .

## B. The $\mathcal{T}_{3,2}$ knot

The technique used to define the wave-function of the trefoil knot can be extended to any other knot built on a torus. The  $\mathcal{T}_{3,2}$  knot can be represented on the torus as shown in Fig. 4. In this case the generic plane  $sOz$  intersects the knot in six points, where the centers are function  $g(\phi)$  of the angle  $\phi$  and rotate around the circumference defined by the plane and the torus intersection. An example of the configuration for  $\phi = 0$  is shown in Fig. 5. The function  $g(\theta)$  is  $g(\theta) = 2\theta/3$ , with  $\phi \in [0, \pi)$ .

Again, using the two-dimensional vortex description  $\Psi_{2D}$ , in the limit of inter-vortex distance much greater than the healing length  $\xi$ , the three-dimensional wave-function of a  $\mathcal{T}_{2,3}$  knot is

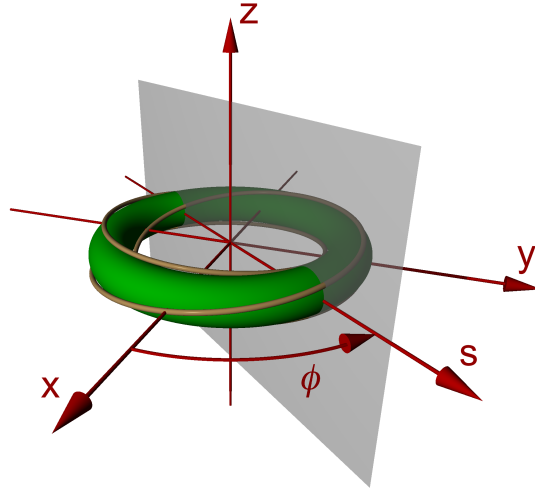


FIG. 4. (Colours online). Construction of the trefoil knot  $\mathcal{T}_{3,2}$ .

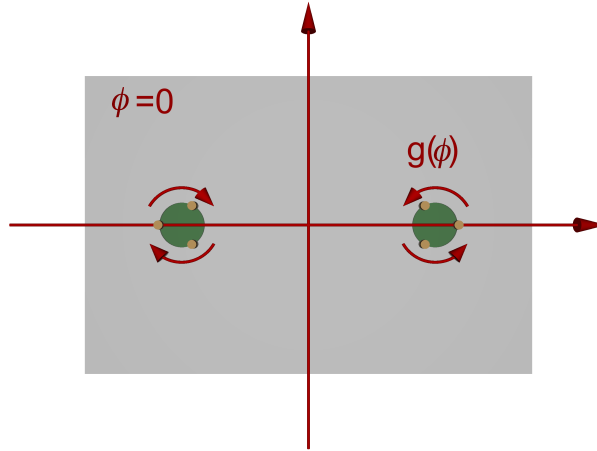


FIG. 5. (Colours online). Positions of the six vortices on  $\phi = 0$  used to construct the wave-function of the trefoil knot  $\mathcal{T}_{3,2}$ .

$$\begin{aligned}
\psi_{3,2}(x, y, z) = & \Psi_{2D} \{s(x, y) - R_0 - R_1 \cos [\alpha(x, y)], z - R_1 \sin [\alpha(x, y)]\} \\
& \times \Psi_{2D} \{s(x, y) - R_0 - R_1 \cos [\alpha(x, y) + 2\pi/3], z - R_1 \sin [\alpha(x, y) + 2\pi/3]\} \\
& \times \Psi_{2D} \{s(x, y) - R_0 - R_1 \cos [\alpha(x, y) + 4\pi/3], z - R_1 \sin [\alpha(x, y) + 4\pi/3]\} \\
& \times \Psi_{2D}^* \{s(x, y) + R_0 + R_1 \cos [\alpha(x, y)], z + R_1 \sin [\alpha(x, y)]\} \\
& \times \Psi_{2D}^* \{s(x, y) + R_0 + R_1 \cos [\alpha(x, y) + 2\pi/3], z + R_1 \sin [\alpha(x, y) + 2\pi/3]\} \\
& \times \Psi_{2D}^* \{s(x, y) + R_0 + R_1 \cos [\alpha(x, y) + 4\pi/3], z + R_1 \sin [\alpha(x, y) + 4\pi/3]\},
\end{aligned} \tag{5}$$

with  $s(x, y) = \text{sgn}(x)\sqrt{x^2 + y^2}$  and  $\alpha(x, y) = 2/3 \arctan (y/x)$ .

### III. VORTEX KNOT DYNAMICS

To study the dynamic and stability of the knots  $\mathcal{T}_{2,3}$  and  $\mathcal{T}_{3,2}$  with different geometries we need to find a compromise between the accessible numerical resolution and the box size: we need to resolve small scales near the vortex cores and, at the same time, minimize the finite size (boundary) effects. We recall that the parameters which identify our vortex knots, the toroidal and poloidal radii  $R_0$  and  $R_1$ , are expressed in units of the healing length  $\xi$ .

We chose to uniformly discretize physical space using a Cartesian grid with steps  $\Delta x = \Delta y = \Delta z = 0.5 \xi$  spanning over the *knot ratios*  $R_1/R_0 = 1/10, 1/5, 2/5, 3/5$ . We expect vortex knots to behave similarly to vortex rings, that is to say we expect that they travel along the direction of the torus axis of symmetry (the  $z$ -axis). Taking our computational constraints into account, we use  $192 \times 192 \times 512$  grid points ( $L_x = L_y = 96 \xi$  and  $L_z = 256 \xi$ ) and the toroidal radius  $R_0 = 20 \xi$ . This choice allows us to have a minimum value of  $R_1 = 2 \xi$  (when  $R_1/R_0 = 1/10$ ), acceptable to observe the small inter-vortex interactions, and a maximum knot size of  $2(R_0 + R_1) = 64 \xi$  (when  $R_1/R_0 = 3/5$ ) which gives tolerable boundary effects. Table I summarizes the simulation parameters.

In order to let the knot travel for the maximum distance in the  $z$  direction, at the start of the calculation ( $t = 0$ ) the vortex knot is centered at the point  $[L_x/2, L_y/2, 2(R_0 + R_1)]$ . With this choice, the knot can propagate for a distance of 3 to  $53/11 \simeq 4.8$  times its maximum size, before hitting the opposite side of the computational domain corresponding to  $z = L_z$ . The GPE is integrated in time using a split-step method with anti-periodic

(reflective) boundary conditions. The integration time step is  $\Delta t = 0.02$  smaller than the fastest linear period  $T_c \simeq 0.032$ . This value allows us to conserve the initial energy and mass up to 3% and 1% respectively in all the simulations. Details on the numerical algorithm can be found in Ref. [18].

Fig. 6 and 7 show the iso-surfaces of the density field corresponding to the threshold value  $\rho_{th} = 0.2$  at the initial conditions and at successive times for the  $\mathcal{T}_{2,3}$  and  $\mathcal{T}_{3,2}$  knots respectively (unstable knots will be discussed in the next section). As expected, vortex knots move along the  $z$ -direction (the axis of symmetry of the torus), but also twist around it. Qualitatively, vortex knots with small knot ratio  $R_1/R_0$  are fast and stable, as they propagate along the  $z$ -direction without breaking. During the evolution, Kelvin waves [8] appear; such waves are visible at the last stages of cases (a), (b), (e), and (f).

In order to quantify the evolution of vortex knots and compare one knot with others, we define the knot center of mass  $\mathbf{r}_{CM} = (x_{CM}, y_{CM}, z_{CM})$  as

$$\mathbf{r}_{CM} = \frac{\int_V \mathbf{r} H(\rho_{th} - |\psi|^2) dV}{\int_V H(\rho_{th} - |\psi|^2) dV}, \quad (6)$$

where  $H(\dots)$  is the Heaviside step function. Fig. 8 and 9 show the  $z$  component  $z_{CM}$  of the knot center of mass (shifted with respect to the initial position) for the  $\mathcal{T}_{2,3}$  and  $\mathcal{T}_{3,2}$  cases respectively. In both cases, knots with smaller knot ratio  $R_1/R_0$  move faster, are more stable and propagate for longer distances before breaking up (a filled symbol at the end of each curve marks the break-up point).

The  $z$  component of the velocity of a vortex knot is estimated by evaluating  $v_z(t) = [z_{CM}(t + \tau) - z_{CM}(t)]/\tau$  (where  $\tau = 4$  for numerical convenience). Fig. 10 and Fig. 11

case	knot ratio	max size	min size	stable
$\mathcal{T}_{2,3} - \mathcal{T}_{3,2}$	$R_1/R_0$	$2(R_0 + R_1)$	$2R_1$	Yes/No
(a) — (e)	1/10	$44\xi$	$4\xi$	Y — Y
(b) — (f)	1/5	$48\xi$	$8\xi$	Y — Y
(c) — (g)	2/5	$56\xi$	$16\xi$	N — N
(d) — (h)	3/5	$64\xi$	$24\xi$	N — N

TABLE I. Vortex knot parameters of  $\mathcal{T}_{2,3}$  and  $\mathcal{T}_{3,2}$  used in the simulations.

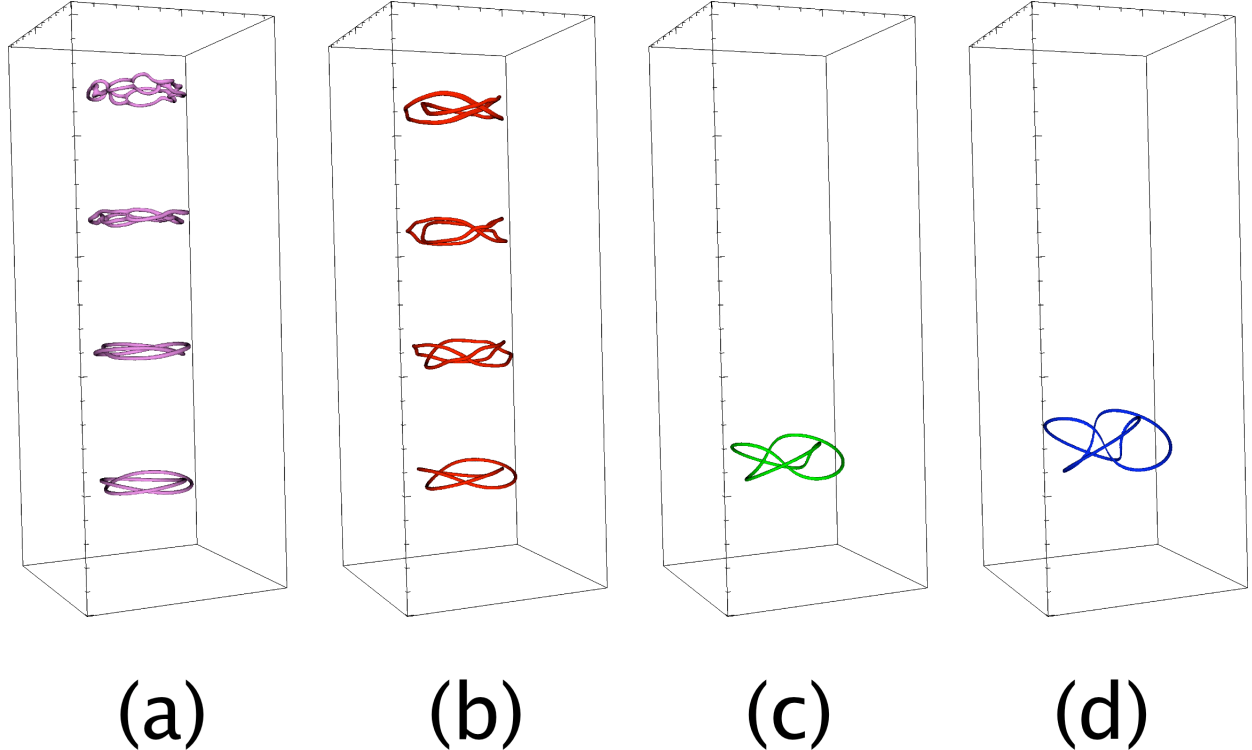


FIG. 6. (Colours online). Iso-surfaces of the density field at the threshold level  $\rho_{th} = 0.2$  for  $\mathcal{T}_{2,3}$  knots of various knot ratios  $R_1/R_0$  (see Table I). Snapshots at times  $t = 0, 400, 800, 1200$ . Unstable knots are not shown.

show  $v_z(t)$  measured in units of the vortex ring velocity [19]

$$v_{\text{ring}}(R) = \frac{n\kappa}{4\pi R} \left[ \ln \left( \frac{8R}{\xi} \right) - 0.615 \right] \quad (7)$$

having quantum number  $n = 1$  and radius  $R = R_0$  (note that in our non-dimensional system the quantum of circulation is  $\kappa = 2\pi$ ). It is apparent that vortex knots move with approximately constant  $z$  velocity before either breaking up or reaching the boundary of the computational domain, where the interaction with the image slows them down.

It is instructive to analyze the mean and the standard deviation of the vortex knots' velocities measured in the constant-velocity regimes. The results, expressed in units of  $v_{\text{ring}}(R_0)$ , are shown in Fig. 12. Three conclusions can be drawn from this figure:

1.  $\mathcal{T}_{2,3}$  knots are slower than  $\mathcal{T}_{3,2}$  knots with the same knot ratio. This is physically expected as the velocity field of torus knots at large distance is similar to the velocity field of vortex rings with multiple circulation:  $\mathcal{T}_{2,3}$  corresponds to circulation of  $2\kappa$  and  $\mathcal{T}_{3,2}$  to  $3\kappa$ . According to Equation (7), the velocity is directly proportional to the

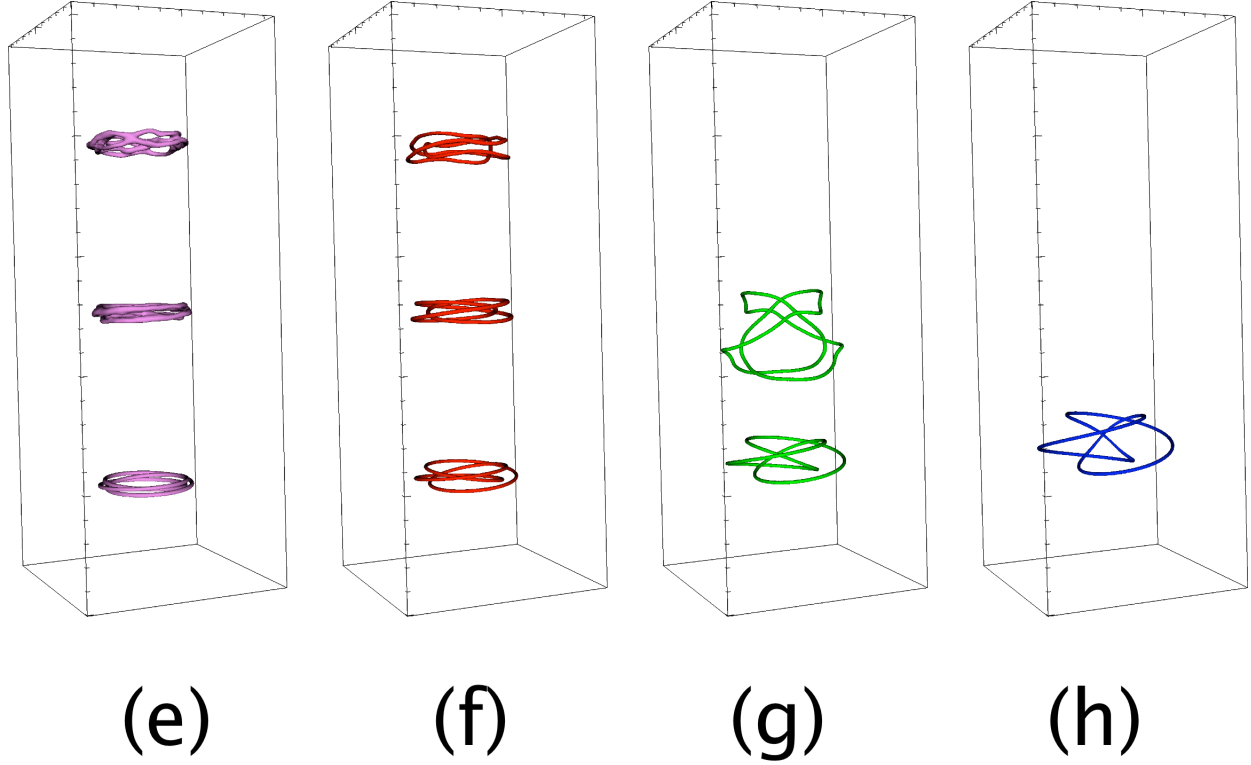


FIG. 7. (Colours online). Iso-surfaces of the density field at the threshold level  $\rho_{th} = 0.2$  for  $\mathcal{T}_{3,2}$  knots of various knot ratios  $R_1/R_0$  (see Table I). Snapshots at times  $t = 0, 400, 800$ . Unstable knots are not shown.

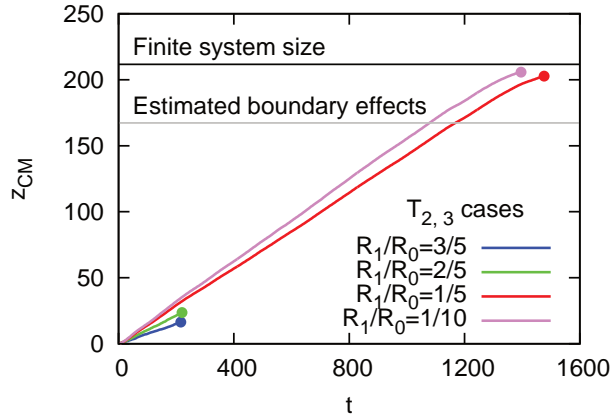


FIG. 8. (Colours online). Position along the  $z$  axis (in units of the healing length) of the centre of mass of  $\mathcal{T}_{2,3}$  knots of various knot ratios  $R_1/R_0$  as a function of time. The filled circles denote the position where vortex knots break up. The horizontal lines denote respectively the distance where boundary effects become non-negligible and the finite system size along  $z$ .

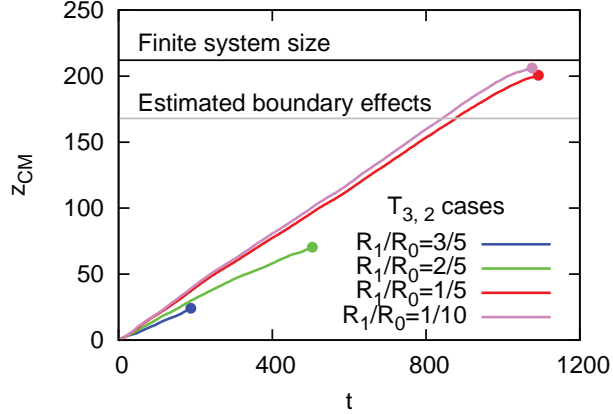


FIG. 9. (Colours online). As in Fig. 8 but for  $\mathcal{T}_{3,2}$ .

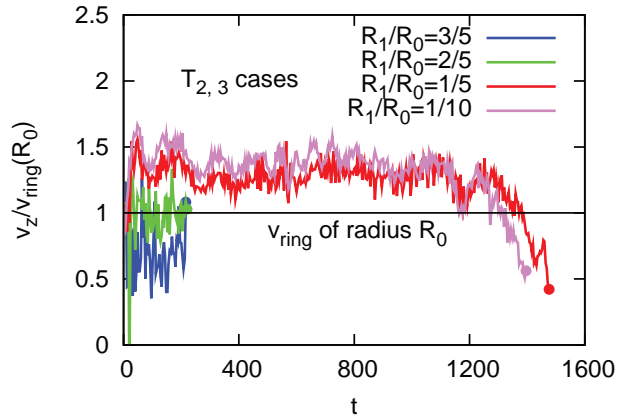


FIG. 10. (Colours online). Velocity component  $v_z$  of  $\mathcal{T}_{2,3}$  versus time of knots with various knot ratios  $R_1/R_0$  before destroying (filled points). Velocities are expressed in units of vortex ring velocity (7) with quantum number  $n = 1$  and radius  $R = R_0$ .

circulation, and so  $\mathcal{T}_{2,3}$  knots should be slower than  $\mathcal{T}_{3,2}$  ones. However, this simple consideration does not apply well to knots because we would have expected, for the small knot ratio tested ( $R_1/R_0 = 1/10$ ) a scaled velocity of  $v_z/v_{\text{ring}}(R_0) \simeq 2$  and  $v_z/v_{\text{ring}}(R_0) \simeq 3$  for  $\mathcal{T}_{2,3}$  and  $\mathcal{T}_{3,2}$  respectively, and this is not the case.

2. The z-velocity component scales with the knot ratio and can be parametrised as

$$v_z \left( \frac{R_1}{R_0} \right) = A_{n,m} \frac{R_1}{R_0} + B_{n,m} \quad (8)$$

where  $A_{n,m}$  and  $B_{n,m}$  are coefficients which refer to the generic torus knot  $\mathcal{T}_{n,m}$ . Values of  $A_{n,m}$  and  $B_{n,m}$  for the knots  $\mathcal{T}_{2,3}$  and  $\mathcal{T}_{3,2}$  are reported in Fig. 12. It is interesting

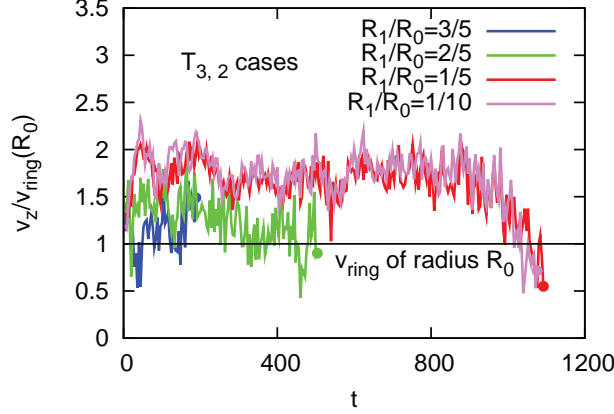


FIG. 11. (Colours online). Velocity component  $v_z$  of  $\mathcal{T}_{3,2}$  knots having different knot ratio  $R_1/R_0$  before destroying (filled points). Velocities are expressed in units of ring velocity (7) having quantum number  $n = 1$  and radius  $R = R_0$ .

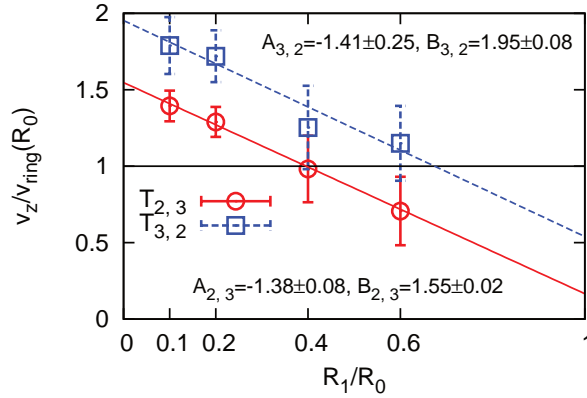


FIG. 12. (Colours online). Averaged velocity components  $v_z$  of  $\mathcal{T}_{2,3}$  and  $\mathcal{T}_{3,2}$  vortex knots with various knot ratios  $R_1/R_0$ . Velocities are expressed in units of vortex ring velocity (7) with quantum number  $n = 1$  and radius  $R = R_0$ ; error-bars correspond to one standard deviation.

to observe that  $A_{2,3} \simeq A_{3,2}$ .

3. The z-velocity component of unstable knots (i.e. knots that decay before reaching the computational boundaries) is less or similar to  $v_{\text{ring}}(R_0)$ . On the contrary, knots that remain stable within the computational domain are characterized by  $v_z > v_{\text{ring}}(R_0)$ .

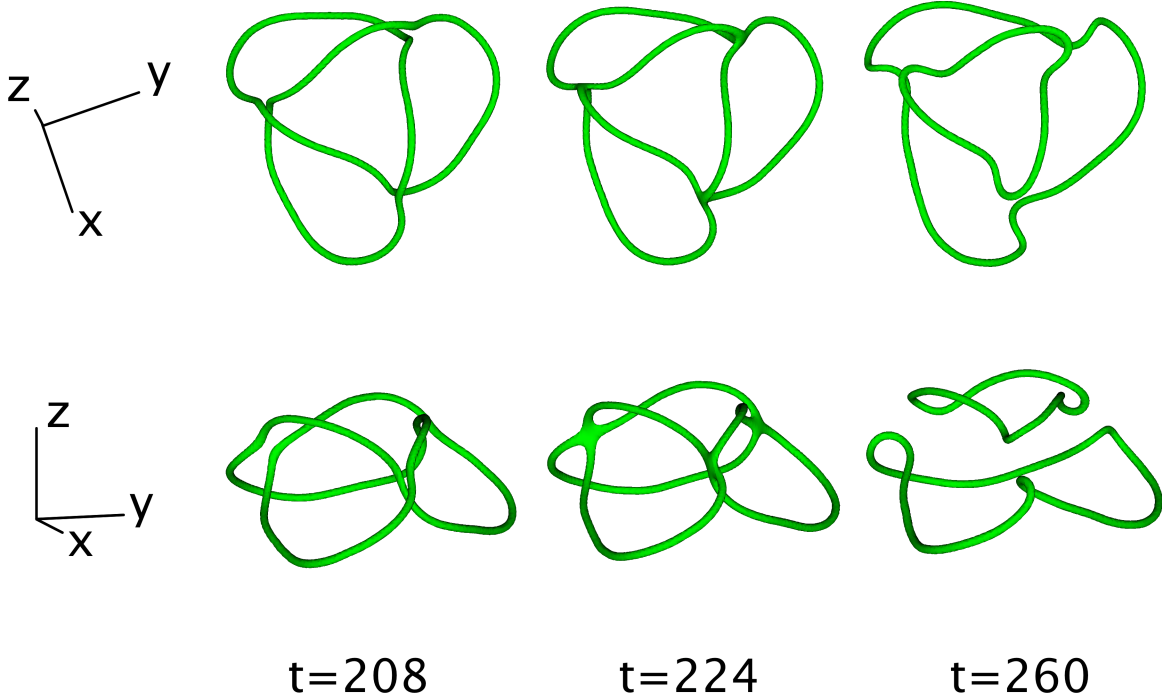


FIG. 13. (Colours online). Three successive snapshots showing how the  $\mathcal{T}_{2,3}$  vortex knot with knot ratio  $R_1/R_0 = 2/5$  breaks up into two vortex rings. Here we plot two perspectives (up and side to the vortex propagation) of the iso-surfaces of the density field corresponding to the threshold level  $\rho_{th} = 0.2$ .

#### IV. THE BREAKING OF A KNOT

In our simulations we have observed that some vortex knots break up into topologically simpler objects.

We first analyze the unstable  $\mathcal{T}_{2,3}$  knots: these are knots corresponding to knot ratios  $R_1/R_0 = 2/5, 3/5$ . In Fig. 13 we show three snapshots of the decay of the  $\mathcal{T}_{2,3}$  knot with ratio  $R_1/R_0 = 2/5$ . It is apparent that the knot breaks into two vortex rings via three simultaneous self-reconnection events (see in particular the snapshot corresponding to  $t = 224$ ). The decay of the vortex knot  $\mathcal{T}_{2,3}$  with ratio  $R_1/R_0 = 3/5$ , not shown here, is similar.

On the contrary,  $\mathcal{T}_{3,2}$  vortex knots break in a different manner. As shown in Fig. 14, the vortex knot  $\mathcal{T}_{3,2}$  with knot ratio  $R_1/R_0 = 3/5$  first decays in one vortex ring and two linked vortex rings via two simultaneous self-reconnection events (snapshot at time  $t = 192$ ). Subsequently, the small free ring escapes from the other rings, which undergo

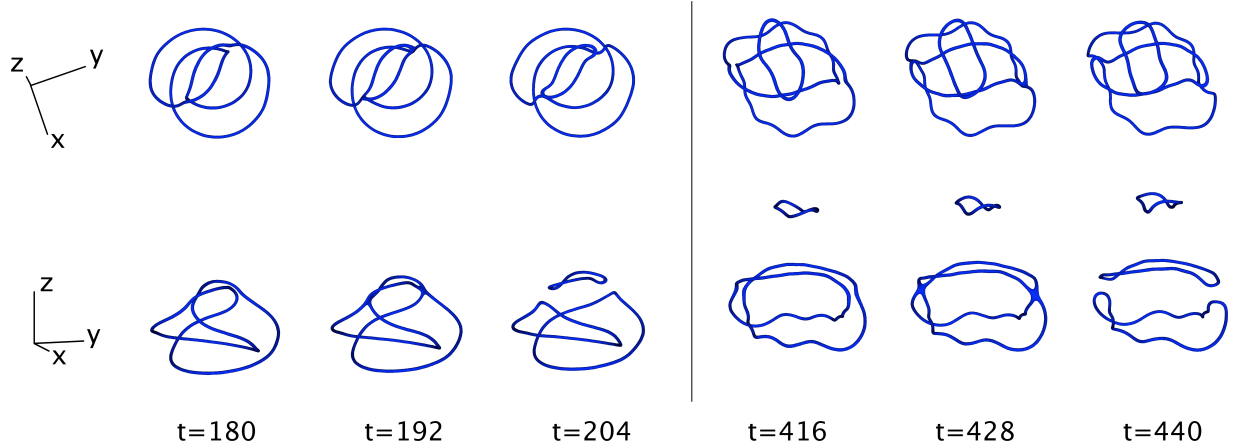


FIG. 14. (Colours online). Two sequences of three successive snapshots showing how the  $\mathcal{T}_{3,2}$  vortex knot with knot ratio  $R_1/R_0 = 3/5$  breaks up into three vortex rings. Here we plot two perspectives (up and side to the vortex propagation) of the iso-surfaces of the density field corresponding to the threshold level  $\rho_{th} = 0.2$ .

two simultaneous reconnection events that create two unlinked vortex rings (snapshot at time  $t = 428$ ). The last step is remarkable: there is no apparent reason why two linked vortex knots should in principle unlink into two vortex rings (by making two simultaneous reconnection events) without forming a single ring (by one reconnection event).

The  $\mathcal{T}_{3,2}$  vortex knot with ratio  $R_1/R_0 = 2/5$  qualitatively decays in the same way, producing a set of three unlinked vortex rings, but the steps are quite different. In the first step, a free vortex ring and two linked vortex rings are again produced. However, the free ring, which is initially located behind the two linked vortex rings, is smaller and faster than the other rings. As a consequence, it reconnects with the two linked vortex rings, as shown in Fig. 15 (snapshot  $t = 752$ ). At this point the reformed knot breaks up, undergoing the same sequence previously described for the  $\mathcal{T}_{3,2}$  with ratio  $R_0/R_1 = 3/5$  case, and the outcome is a set of three vortex rings (snapshot at time  $t = 952$ ). Note that, in the last snapshot, the first knot (in the sense of the position) has split into two smaller vortex rings via a self-reconnection event which is probably consequence of its Kelvin waves oscillations.

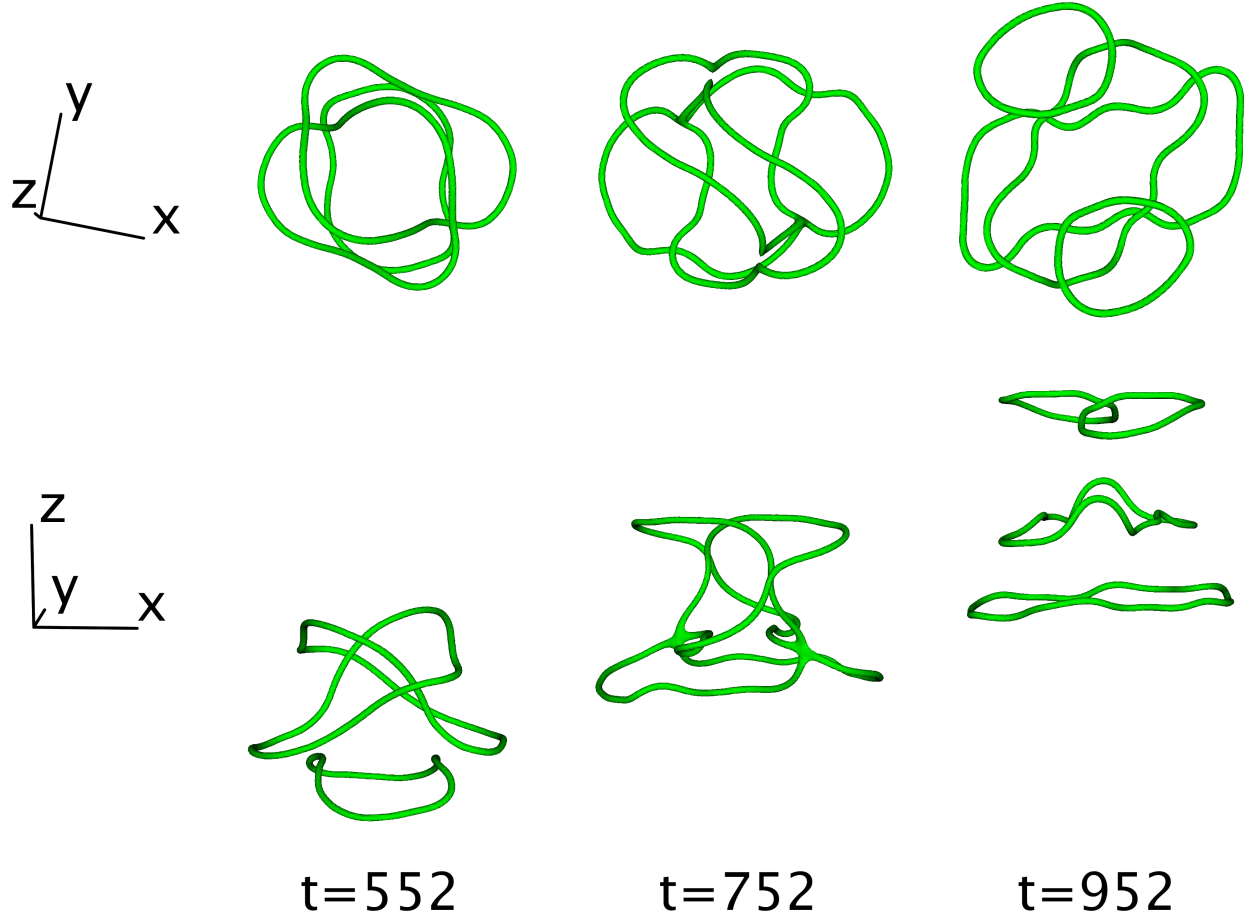


FIG. 15. (Colours online). Three successive snapshots showing how the  $\mathcal{T}_{3,2}$  knot with knot ratio  $R_1/R_0 = 2/5$  breaks into three vortex rings. Here we plot two perspectives (up and side to the vortex propagation) of the iso-surfaces of the density field corresponding to the threshold  $\rho_{th} = 0.2$ .

## V. CONCLUSIONS

We have numerically analyzed the existence and stability of vortex knots in the GPE model of a condensate. We have proposed a novel numerical technique for creating *ab initio* vortex knots in the wave-function of the condensate. In particular, we have focussed our numerical computations on the two simplest (in the topological sense) vortex knots,  $\mathcal{T}_{2,3}$  and the  $\mathcal{T}_{3,2}$ . We have analyzed the evolution and the stability of such knots with respect to the knot ratio  $R_1/R_0$ . We have found that a knot can be unstable, i.e. it breaks up into simple rings during the propagation, or stable within our computational domain. Our numerical experiments clearly show that a small knot ratio ( $R_1/R_0 = 1/10, 1/5$ ) increases the stability,

whereas a large knot ratio ( $R_1/R_0 = 2/5, 3/5$ ) decreases it, in agreement with [12].

We have found that vortex knots propagate essentially as vortex rings. We have measured the vortex knot velocities along the torus symmetry axis and shown that the velocity depends linearly on the knot ratio for both  $\mathcal{T}_{2,3}$  and  $\mathcal{T}_{3,2}$ .

Finally, we have studied the details of the break up of vortex knots. Although we do not have a theoretical explanation for the break up, we have observed evidences of generic breaking behavior:  $\mathcal{T}_{2,3}$  knots always break into two vortex rings via a three simultaneous self-reconnection event, whereas.  $\mathcal{T}_{3,2}$  knots first decay into three vortex rings via two simultaneous self-reconnections which create a free ring and two linked rings, then undergo two simultaneous reconnections which split the resulting link.

We believe that our work opens up new interesting problems in the field of fluid topology applied to superfluids and Bose-Einstein condensates. The natural developments of our study will be a theoretical investigation of the stability of vortex knots, and an experimental study of the creation of a knotted initial condition in an atomic condensate.

## ACKNOWLEDGMENTS

The authors acknowledge G. Boffetta, F. De Lillo, A.L. Fetter and A.J. Youd for comments and suggestions. CFB is grateful to the Leverhulme Trust for financial support. The authors also thank developers at *LLNS VisIt*, *POV-Ray* and *Gnuplot* for the free software used for the visualization of numerical results.

- 
- [1] W. H. Thomson, Transactions of the Royal Society of Edinburgh, **25**, 217 (1869).
  - [2] C. Adams, *The knot book* (WH Freeman, 1994).
  - [3] P. M. Sutcliffe and A. T. Winfree, Phys. Rev. E, **68**, 016218 (2003).
  - [4] L. Faddeev and A. J. Niemi, Nature, **387**, 58 (1997).
  - [5] J. Leach, M. R. Dennis, J. Courtial, and M. J. Padgett, Nature, **432**, 165 (2004), ISSN 0028-0836.
  - [6] M. R. Dennis, R. P. King, B. Jack, K. O’Holleran, and M. J. Padgett, Nat Phys, **6**, 118 (2010), ISSN 1745-2473.

- [7] U. Tkalec, M. Ravnik, S. Copar, S. Zumer, and I. Musevic, *Science*, **333**, 62 (2011), <http://www.sciencemag.org/content/333/6038/62.full.pdf>.
- [8] R. Donnelly, *Quantized vortices in Helium II*, Vol. 3 (Cambridge Univ Pr, 1991).
- [9] P. M. Walmsley and A. I. Golov, *Phys. Rev. Lett.*, **100**, 245301 (2008).
- [10] B. P. Anderson, P. C. Haljan, C. A. Regal, D. L. Feder, L. A. Collins, C. W. Clark, and E. A. Cornell, *Phys. Rev. Lett.*, **86**, 2926 (2001).
- [11] D. R. Poole, H. Scofield, C. F. Barenghi, and D. C. Samuels, *Journal of Low Temperature Physics*, **132**, 97 (2003), ISSN 0022-2291, 10.1023/A:1023797226059.
- [12] R. Ricca, D. C. Samuels, and C. F. Barenghi, *J. Fluid Mech.*, **391**, 29 (1999).
- [13] F. Maggioni, S. Alamri, C. F. Barenghi, and R. L. Ricca, *Physical Review E*, **82**, 026309 (2010).
- [14] L. Pitaevskii and S. Stringari, *Bose-Einstein Condensation*, Vol. 116 (Oxford University Press, USA, 2003).
- [15] Saffman, P. G., *Vortex Dynamics* (Cambridge University Press, Cambridge, 1991).
- [16] J. Koplik and H. Levine, *Phys. Rev. Lett.*, **71**, 1375 (1993).
- [17] N. Berloff, *Journal of Physics A: Mathematical and General*, **37**, 1617 (2004).
- [18] D. Proment, S. Nazarenko, and M. Onorato, *Physica D: Nonlinear Phenomena*, (2011), ISSN 0167-2789.
- [19] P. Roberts and J. Grant, *Journal of Physics A: General Physics*, **4**, 55 (1971).